

# Predicting and Accelerating Nanomaterials Synthesis Using Machine Learning Featurization

Christopher C. Price,<sup>\*,†</sup> Yansong Li,<sup>‡</sup> Guanyu Zhou,<sup>‡</sup> Rehan Younas,<sup>‡</sup> Spencer S. Zeng,<sup>†</sup> Tim H. Scanlon,<sup>†</sup> Jason M. Munro,<sup>\*,†</sup> and Christopher L. Hinkle<sup>\*,‡</sup>

<sup>†</sup>*Atomic Data Sciences, Boston, Massachusetts 02116, United States*

<sup>‡</sup>*Department of Electrical Engineering, University of Notre Dame, Notre Dame, Indiana 46556, United States*

E-mail: chris@atomicdatasciences.com; jason@atomicdatasciences.com; chinkle@nd.edu

## Abstract

Solving for the complex conditions of materials synthesis and processing requires analyzing information gathered from multiple modes of characterization. Currently, quantitative information is extracted serially with manual tools and intuition, constraining the feedback cycle for process optimization. We use machine learning to automate and generalize feature extraction for in-situ reflection high-energy electron diffraction (RHEED) data to establish quantitatively predictive relationships in small sets ( $\sim 10$ ) of expert-labeled data, and apply these to save significant time on subsequent epitaxially grown samples. The fidelity of these relationships is tested on a representative material system ( $W_{1-x}V_xSe_2$  growth on c-plane sapphire substrate (0001)) at two stages of synthesis with two aims: 1) predicting the grain alignment of the deposited film from the pre-growth substrate surface data, and 2) estimating the vanadium (V) dopant concentration using in-situ RHEED as a proxy for ex-situ methods (e.g. x-ray photoelectron spectroscopy). Both tasks are accomplished using the same set of

materials agnostic core features, eliminating the need to retrain for specific systems and leading to a potential 80% time saving over a 100 sample synthesis campaign. These predictions provide guidance for recipe adjustments to avoid doomed trials, reduce follow-on characterization, and improve control resolution for materials synthesis, ultimately accelerating materials discovery and commercial scale-up.

## Introduction

Differentiated and substantial performance requirements for emerging electronics applications and the deceleration of Moore’s Law in silicon is driving demand for advanced materials discovery, optimization, and scale-up.<sup>1</sup> Engineering and development of materials platforms is difficult and time consuming; lab-to-production timelines currently take 10 years or longer, and time-to-market is the primary barrier to commercialization.<sup>2</sup> Significant progress has been made leveraging ab-initio physical simulations (DFT)<sup>3,4</sup> and subsequent machine learning (interatomic potentials;<sup>5-7</sup> generative models<sup>8,9</sup>) to efficiently identify and screen stable and synthesizable materials candidates in the first stage of advanced materials development. However, the theoretical assumptions of DFT, including the absence of constraints relevant to synthesis in the real world, results in a large time and effort barrier to the realization of materials after promising targets are identified.<sup>10</sup> While computational capabilities have taken off, working through synthesis recipe design, process optimization, and iteratively improving materials quality relies on a relatively slow manual and intuition-guided experimental approach. To address this bottleneck, recent efforts in both software and hardware have made advancements towards fully autonomous synthesis and optimization within the lab.<sup>11-14</sup> Advanced tools in machine learning and artificial intelligence have proven incredibly useful at targeting both interpretation of experimental data, and the subsequent decision making required as part of feedback loop-based solutions.<sup>15-17</sup> The early versions of these autonomous systems have emphasized the importance and challenges of effective and rapid materials characterization.

The primary barrier for synthesis optimization is time, and this is magnified when engineering precision is required at the nanoscale. While ultra-high vacuum techniques like molecular beam epitaxy (MBE) have highly controlled synthesis environments, the preparation, processing, and subsequent characterization of a single sample takes multiple days.<sup>18</sup> Synthesis recipes are highly sensitive, varying across equipment installations and requiring re-calibration after tool maintenance, which can extend over weeks. Due to the expense in time and resources consumed per run, it is critical to maximize the information gained and chance of success for each trial in both manual and autonomously driven settings. In-situ characterization captures large volumes of abstract data with high granularity, yet this data cannot be analyzed with conventional methods in time to impact a trial in progress. An example is RHEED, frequently used to qualitatively monitor MBE growth<sup>19</sup> by providing information on the surface structure of a sample. RHEED images contain a fingerprint of the material surface at a point in time that can take 15 minutes to manually extract for a single image, while processes can change in seconds and data is generated 10 to 100 times per second. Recent work has shown that machine learning can process RHEED data,<sup>20–26</sup> but these early demonstrations required manual tuning of hyperparameters, fitting to specific materials systems or camera settings, or delivery of results after the run is completed. While providing significant post-run insights, these attributes hinder the general predictive capacity to modify or reduce the number of trials in synthesis optimization, since they require significant system-specific data to be acquired up front.

In this work, we develop and demonstrate fully automated and general pipelines using both supervised and unsupervised machine learning models to rapidly extract rich and holistic quantitative fingerprints from RHEED data. We show that these fingerprints can speed up the synthesis feedback loop by constructing predictive models from small datasets ( $\sim 10$  samples) of labeled trials to provide relevant feedback from ex-situ analysis using only in-situ inputs. These predictive models are demonstrated in two stages of the synthesis process for the target system, two-dimensional (2D) V-doped  $\text{WSe}_2$  on  $\text{Al}_2\text{O}_3(0001)$  (sap-

phire): 1) evaluating the probability of a substrate to produce grain-aligned film growth, and 2) estimating the composition of a dopant in the film before ex-situ x-ray photoelectron spectroscopy (XPS) is conducted. For both objectives, the success of the predictive models can save significant time and cost by avoiding doomed trials and reducing the number of steps required to assess the sample. By producing these empirically derived predictions for near-real-time feedback, we show that the synthesis optimization loop can be accelerated, leading to higher throughput of material samples with the target characteristics.

## Results and Discussion

Precise doping control in 2D materials is a difficult but necessary milestone to achieve for the next generation of power and space efficient semiconductors. Vanadium doping in  $\text{WSe}_2$  gives p-type doping with spin polarization, making this system a candidate as a high-mobility dilute magnetic semiconductor.<sup>27,28</sup> It is crucial to control the dopant concentration during co-deposition of V and W to minimize domain formation, the key challenge in this materials system. Illustrating the limitations of theoretical prediction, reliably synthesizing theoretically stable, uniformly distributed phases requires high-fidelity control of the kinetics connecting the input procedure to the resulting material composition and microstructure. End-to-end, each trial to map out these relationships can consume over 24 combined hours of tool and active operator time, even excluding the time required for sample loading and equipment standby (Fig. 1a). Here, we develop a general framework that can be used to avoid doomed trials and map ex-situ measurements to in-situ characterization in molecular beam epitaxy to save 80% of the time over a 100 trial synthesis campaign.

### Automated Data Workflows in the Synthesis Context

The data workflow for automated characterization analysis is given in Fig. 1b. RHEED data is transferred to a centralized database which groups each piece of input data by the

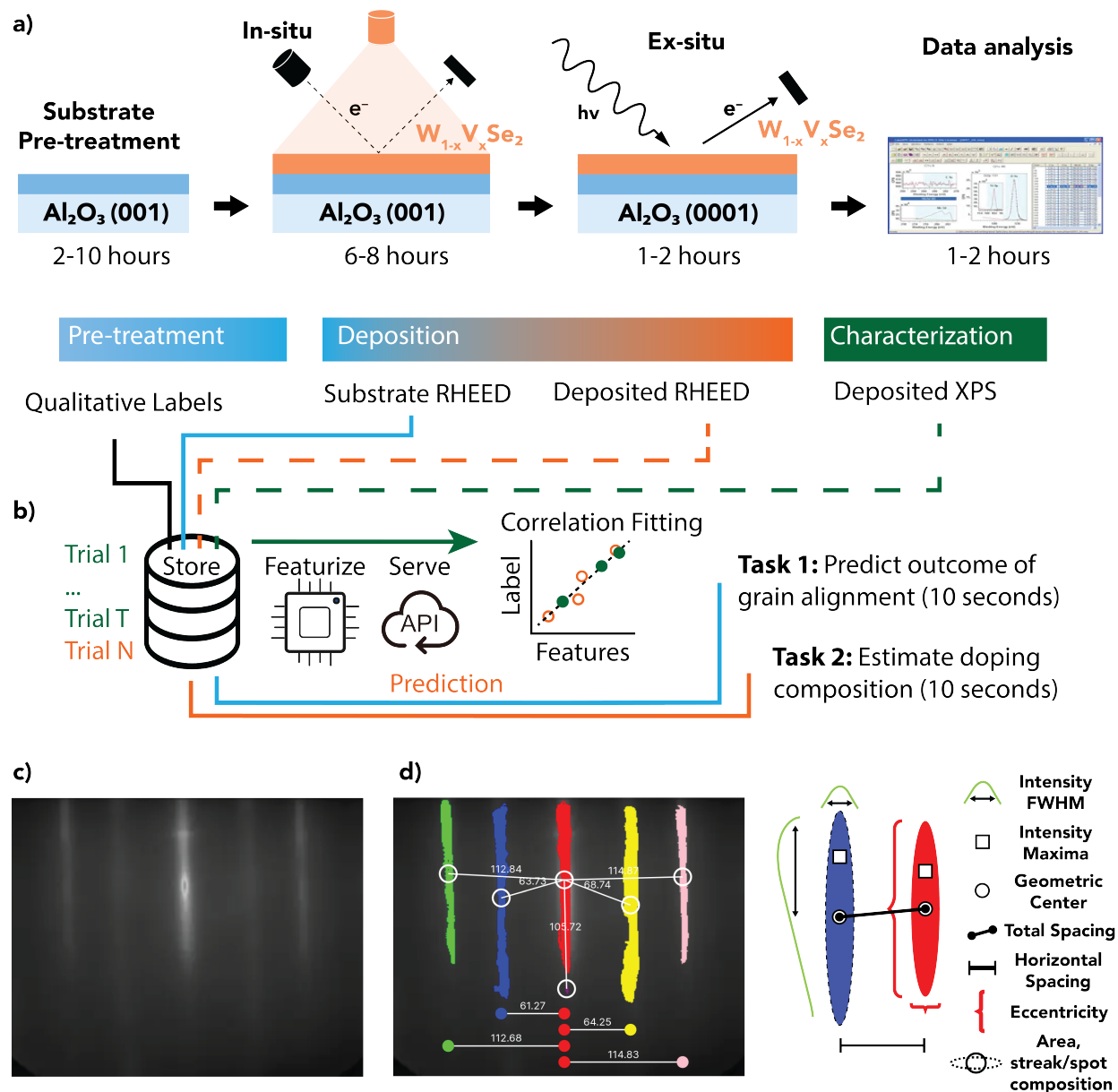


Figure 1: (a) Summary of experimental flows for sample preparation, film growth, and characterization. At the beginning and end of MBE deposition, in-situ RHEED is collected and automatically fingerprinted. After synthesis, the sample is transferred to a separate tool for XPS characterization. (b) Summary of flows for synthesis and characterization data. Labeled trials are iteratively updated in the database, and correlation fitting is performed for the two tasks against the input labels. Next-trial predictions are generated within 10 seconds. (c) An image of a RHEED pattern of the as-grown film, and (d) the featurized fingerprint extracted from the image, including the segmented regions of non-zero intensity. Quantities for each diffraction feature extracted into the fingerprints, which are input to the empirical correlation models.

sample that it corresponds to via a user interface. The two designated tasks are 1) predicting whether a growth is likely to lead to aligned or randomly oriented grains (textured growth) based on the RHEED image of the substrate wafer before deposition starts, and 2) estimating the Vanadium doping composition in a deposited film using a RHEED snapshot as input. These tasks were designed to solve real challenges encountered over a three-year period of aiming to synthesize high quality samples in this material system. Qualitative labels on grain orientation and the quantitative results of manual XPS analysis are added to the central database for the fully analyzed training samples from initial trials  $T = 1$  to  $T_{task}$ , ( $T_1 = 14, T_2 = 8$ ). The input RHEED images are passed through a featurization pipeline which extracts, normalizes, and labels diffraction features categorized in Fig. 1d. Featurization proceeds by cropping the image to remove artifacts from the detector and an image segmentation pipeline composed of two models – a U-Net architecture for RHEED proposed by Liang *et al.*<sup>20</sup> followed by a transformer-based segmentation model<sup>29</sup> tuned for performance on low-contrast medical grayscale images.<sup>30</sup> The original RHEED pattern in Fig. 1c shows typically diffuse and subtle scattering features that need to be separated from the background, highlighting the challenges of manual analysis and the need for task-specific models and model combinations for high-fidelity results. Output masks from this segmentation pipeline are labeled to identify contiguous diffraction regions and the quantified features are computed for each diffraction node (Fig. 1d). A coordinate system using the specular spot as the origin is adopted to enable comparison of diffraction features across patterns collected under different conditions. In the featurization scheme, no hyperparameters are input or adjusted across different patterns or materials systems to maximize generalizability and enable real-time result generation without intervention. The featurized RHEED datasets take 10 seconds to generate per frame, and are served through an application programming interface (API) to generate predictions from the correlative models derived from the task specific training samples; details in the **Methods** section.

# Independent Classification of Film Crystallinity from Film and Substrate RHEED

Given the critical role of crystallinity in material synthesis and downstream device performance, our first task is to classify and predict the eventual grain alignment of deposited films based on in-situ RHEED characterization. In the case of 2D chalcogenide growth, epitaxial alignment is particularly susceptible to the surface topography of the sapphire substrate.<sup>31</sup> Surface reconstructions ( $1 \times 1$  Al-terminated or  $(\sqrt{31} \times \sqrt{31})R9$ ) supporting aligned growth are achieved by thermal annealing, but significant variance in the results exists due to coupling of the annealing procedure with the individual wafer and furnace conditions. Evaluating whether a substrate will lead to aligned grains prior to deposition, and if a deposited film is aligned, can avoid doomed efforts that lead to low quality samples and save time. Figure 2 shows the classification results based on the featurized RHEED datasets and an initial label set from visual inspection which placed as-grown films in either a textured or aligned category. Fig. 2a shows examples of strongly aligned (top) and textured (bottom)  $\text{WSe}_2$  films, and Fig. 2b-c gives the baseline classification results for the deposited  $\text{WSe}_2$  films. The classifier is a logistic regressor wrapped with bootstrap aggregation (bagging), a technique that resamples the training data with replacement to get an overall model less prone to overfitting. We restrict to small training datasets to mimic the typical data availability in the early stages of a synthesis effort and maximize the ability to provide guidance for a subsequent trial. The confusion matrix in Fig. 2b gives the binary grain alignment prediction accuracy of 80%; further details of the bagging procedure are given in **Methods**. The classification probabilities for grain-aligned films are plotted in Fig. 2c along with the misclassification frequency for each sample. The probability of classification serves as an uncertainty metric and a quantitative approximation for the degree of overall grain alignment. Some samples are always misclassified when held out of the training set, including the canonically textured film 9. This is a limitation of the small dataset size; when film 9 is not included in fitting, the signal identified to correlate with textured films changes signif-

icantly. This highlights the importance of including strong examples of target phenomena in the fitting set, and the strength of the correlative approach to interpolate and provide guidance on examples that are ambiguous. Overall, the results indicate that the RHEED features contain enough signal to automatically match the expert-identified trends in the labels with a small set of examples. Automating this task removes operator bias from data analysis, and quantification helps set thresholds for films which meet the quality criteria for subsequent device fabrication. However, additional operator time, tool time, and resources could be saved by avoiding low quality film growths before they occur.

Natural variance with substrates and precursors can lead to unexpected growth outcomes, even if the same recipe is programmatically followed; in this WSe<sub>2</sub> system deposition alone consumed up to 8 hours, and average all-in synthesis times can range from 5 to 14 hours for MBE.<sup>32</sup> Using the same data infrastructure and feature extraction as for the WSe<sub>2</sub> films, we perform an identical fitting procedure using the pre-deposition sapphire RHEED patterns as inputs instead of the as-grown films, with results in Fig. 2d-f. Fig. 2d similarly shows the different surface reconstructions of the sapphire that can lead to aligned (top) or textured (bottom) growth. The logistic regression classifier with bootstrap aggregation achieves an accuracy near 80%, similar to the results from the WSe<sub>2</sub> RHEED, although the most-misclassified samples differ than those using the film RHEED. For the misclassified samples in Fig. 2c, the quantitative probability score is close to 50%, indicating greater uncertainty of prediction. We show that the quantitative classification probability for both datasets correlates with qualitative assessment with a detailed view of sample 12 in Fig. S1; this sample is labeled as grain-aligned but shows a lower classification probability for both the substrate and the film. In the sapphire RHEED data for sample 12, several features of the  $(\sqrt{31} \times \sqrt{31})R9$  reconstruction are missing compared to the aligned-producing substrate 7, and the Kikuchi lines are better matched with the textured-generating substrate of sample 9. In the as-deposited film, the pattern is consistent with an aligned growth, but there are identified small features that are signatures of the textured films. This indicates that the



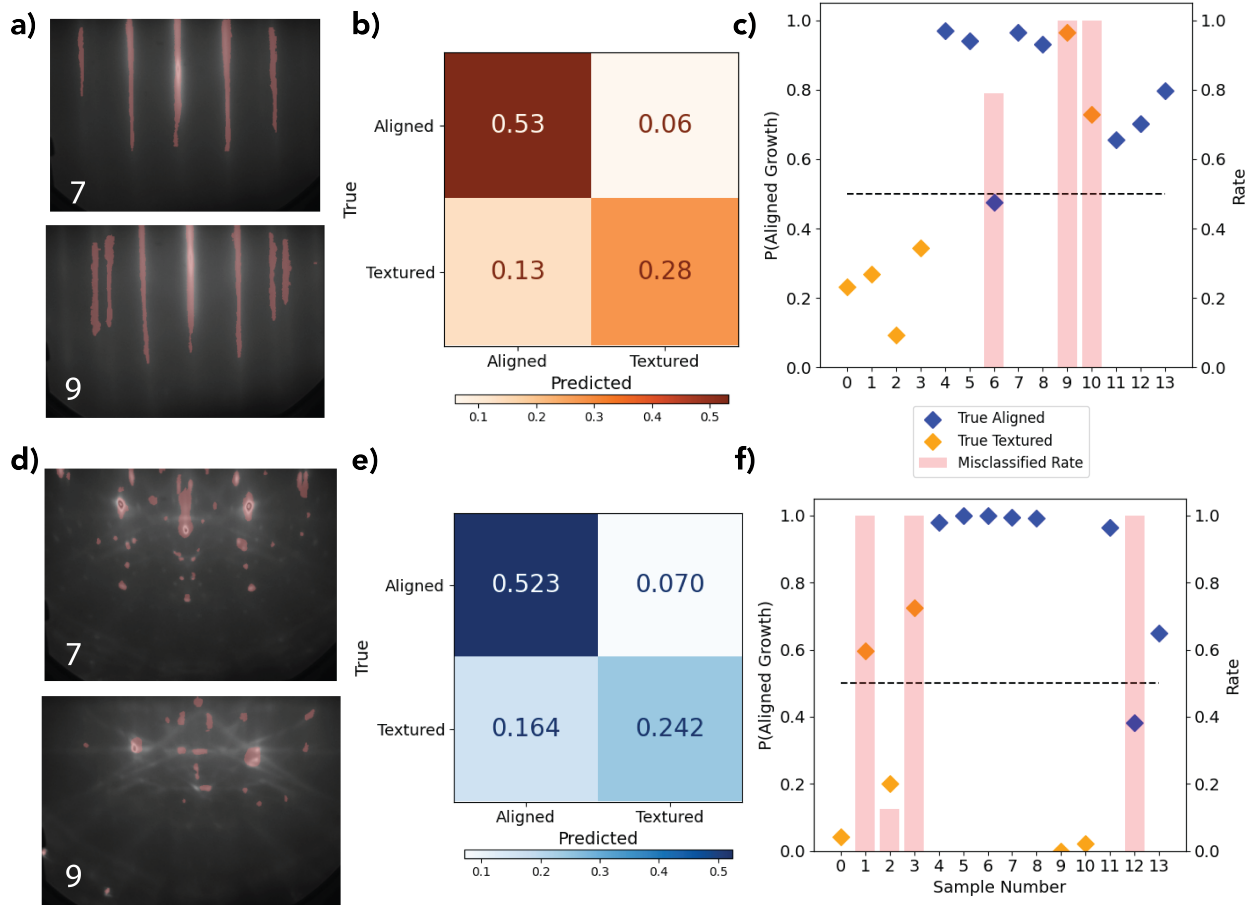


Figure 2: Figure 2: (a) Segmented RHEED patterns for examples of aligned (top) and textured (bottom) WSe<sub>2</sub> film growth. Labels in the bottom left correspond to sample number. (b) Confusion matrix and classification accuracy for a logistic regression model fit with bootstrap aggregation to a set of 14 samples of featurized WSe<sub>2</sub> patterns. (c) Probability of aligned growth predictions by sample (scatters) and frequency of misclassification (bars) for the WSe<sub>2</sub> RHEED data. (d) Segmented RHEED patterns for examples of sapphire substrates that led to aligned (top) and textured (bottom) film growths. (e) Confusion matrix and classification accuracy for the same model structure in (b), fit to the substrate RHEED instead of the film RHEED against the film labels. (f) Same as (c) for the sapphire substrate pattern classification task.

classification probability contains some information about the quantified degree of likely grain alignment from the substrate that appears in the deposited film, providing a new resource for decision making on whether to proceed with a growth on a given pre-treated substrate. If the likelihood of achieving high-quality growth is deemed low, researchers have the option to either perform additional pre-growth treatments or switch to a different substrate, rather than proceeding with what may be a fruitless attempt.

## Mapping Ex-Situ Measured Composition to In-Situ RHEED

With a roadmap established to improve the yield of film growth with the correct microstructure, we turn to optimization and control of film composition by estimating dopant concentration without removing the sample from the growth chamber. Conventionally, dopant concentrations are determined ex-situ by characterization techniques like XPS and energy-dispersive x-ray spectroscopy (EDX) after the entire growth session, requiring time-consuming sample relocation. The scattering factors of different elements create intensity modulations and shifts in the RHEED pattern, but this information is difficult to assess directly since it is tightly convolved with other diffraction mechanisms.<sup>33-35</sup> If compositional feedback can be quickly generated and delivered from in-situ inputs like RHEED, it would allow for finer and immediate control over compositional doping and make adjustments to a sample during processing. The relationships between composition, tool parameters, and growth recipe are nonlinear for even highly controlled synthesis environments such that fully mapping design space requires extensive trial and error. If compositional feedback can be quickly generated and delivered from in-situ inputs, it becomes possible to have finer control over compositional doping and make adjustments to a sample during processing.

Figure 3 presents a design of experiments simulating the early stages of a synthesis campaign for the model system ( $W_{1-x}V_xSe_2$ ) with the goal of assessing the vanadium doping composition in-situ. Labels are drawn from XPS analysis of the V-2p peak (Fig. 3d). The initial training set of labeled examples corresponds to two undoped films, a sample measured

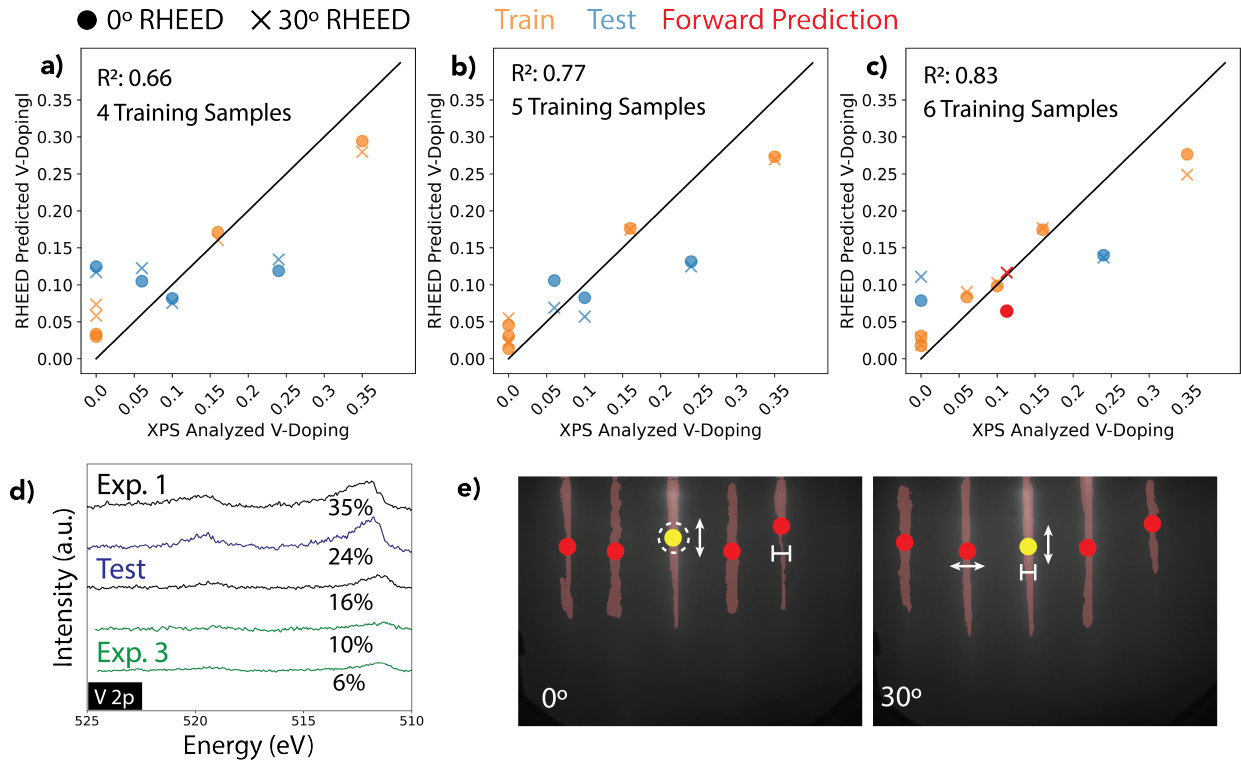


Figure 3: Figure 3: (a-c) Predicted vs. actual plots for vanadium doping composition in  $W_{1-x}V_xSe_2$  assessed by XPS measurement (x-axis) and predicted from RHEED features (y-axis) across a simulated design of experiments from  $T = 4$  to  $T = 6$ . Orange points are used for fitting the RHEED proxy models, blue points are test data; dots and x's show predictions made from two high symmetry RHEED angles. In (b) and (c), a random test point is added to the training set to simulate another sample growth. The quality of the RHEED prediction increases with each additional sample. Red points in (c) indicate freshly grown sample prediction. (d) XPS data used to generate the labels for each sample. (e) Interpretation of the model predictions; the features with the largest coefficients are the relative specular spot intensity maxima location, the relative position of the first order spots, and the width of the second order spots.

at  $x=0.16$ , and a sample measured at  $x = 0.35$  (Fig. 3a, orange). This corresponds to the limits of the desired doping window and the midpoint. Due to the minimally small number of labeled samples, we apply linear regression with bootstrap aggregation to look for correlations between the featurized RHEED and the XPS quantification while minimizing overfitting. The blue points show the predictions for samples held out of the fitting to simulate forward prediction in a real synthesis scenario, with the XPS derived labels on the x-axis. Points that fall on the black line indicate a perfect match between the XPS composition result and the RHEED-predicted composition result, and the  $R^2$  value in the top left quantifies the average agreement across all of the training and testing samples. In panel **b** (c), one (two) test point(s) is (are) added into the training set to measure the change in model performance with additional samples labeled with XPS. Identical fitting procedures were conducted on two independent RHEED series collected on the same samples but at two different azimuthal angles separated by  $30^\circ$  (dots and x's) to reduce the likelihood that identified correlations are due to artifacts of data collection. The red point in Fig. 3c represents the prediction on a brand new sample excluded from all training and testing recently synthesized to test the efficacy of true forward prediction and remove implicit bias - details in Fig. S2.

Using a design-of-experiments approach, where samples at the endpoints and midpoint of the target composition range are collected first and labeled with XPS, we show that substantial predictive capability can be uncovered from a small initial dataset. From figure 3a-c, the accuracy of V-composition prediction increases with each additional fitting point. There are no substantially outlying predictions, a point which is important in practice for using these models as surrogates for ex-situ characterization and in-chamber guidance. Across the three scenarios of training and testing, there is substantial agreement in the resulting predictions from both angles of RHEED collection, indicating that the V-doping correlated scattering changes are reliable and not an artifact of data collection. The predictions for the three undoped films, while non-zero and non-uniform, preserve the relative trend in composition and are clustered together among three distinct samples. We interpret the features that

contribute the most to the model correlation using the magnitude of the slope coefficients averaged over the bootstrapped estimators (Fig. 3e). In panel (e), the most important features for each angle are shown - the relative location of the intensity maxima within the specular spot, the width of several of the first and second order diffraction features, and the area of the specular region classified as spot-like.<sup>20</sup> Feature importance is an entrypoint for deeper physics-based data analysis, indicating where non-random variance is greatest and consequently which structural mechanisms may be correlated with the target property.

## Conclusions

We demonstrate that machine learning models tailored for RHEED data can be used to extract high-fidelity feature sets that reveal rich relationships across materials systems within small sets of supplied labels. The predictions from these trained models can be used to avoid synthesis trials likely to fail based on substrate conditions, reduce the amount of ex-situ characterization work, and provide real-time feedback on properties not traditionally accessible in the synthesis environment. Since the number of samples for an individual research project can be on the order of hundreds, and fine tuning materials processing to improve yield can be on the order of many thousands, the delivery of these predictions using dedicated data infrastructure can potentially save thousands of expert hours in material preparation and data analysis.

## Methods

### Sapphire Substrate Treatment

2-inch *c*-plane sapphire substrates (0001) (Cryscore) with intentional miscut of C off A by 0.2° were pre-growth annealed at 1200 °C for 5 hours in a tube furnace (Thermco Furnace) inside a class 100 cleanroom. During the annealing, the nitrogen gas continuously flowed at

3 L/min through the furnace under atmospheric pressure.

### **Vanadium-doped WSe<sub>2</sub> Thin Film Growth**

The W<sub>1-x</sub>V<sub>x</sub>Se<sub>2</sub> thin films were grown on the pre-treated *c*-plane sapphire substrates (Cryscore) in an MBE system (Scienta Omicron) with a base pressure of  $\tilde{1}0^{-10}$  mbar. Prior to the deposition, the sapphire substrate was degassed at 900 °C for 1 hour. Then the thin films were grown at 550 °C by co-depositing V from an effusion cell, Se evaporated from an effusion cell with a cracker zone, and W from an electron-beam evaporator. A relatively high Se flux of  $1.0 \times 10^{-6}$  mbar, measured by beam flux monitor, was used to minimize Se vacancies in the films. After the co-deposition, the samples were still exposed to the same Se flux and annealed at 700 °C for 2 hours. To monitor the growth process, in-situ RHEED (Scienta Omicron) was operated with an acceleration voltage of 13 kV and a current of 1.48 A.

### **X-ray Photoelectron Spectroscopy**

After growth, the samples were transferred directly to the integrated XPS chamber without breaking the vacuum. XPS measurements were carried out using an Al K- $\alpha$  X-ray source (1486.7 eV) under a background pressure of  $2.6 \times 10^{-9}$  mbar. An electron neutralizer was turned on during the measurement to compensate for charging effects caused by the insulating sapphire substrate.

### **Data Analysis**

RHEED featurization datasets were generated using AtomCloud RHEED analysis software and accessed via API for training and inference. Correlation models are taken from the scikit-learn python package. For substrate classification and inference, principal component analysis (PCA) is performed on the training dataset, and bootstrap aggregation with 100 estimators is used around a base logistic regression, with metrics averaged over 128 independent trials with different held out data. The same fit components are used to trans-

form data for inference. For dopant composition estimation, no PCA preprocessing is used before bootstrap aggregation around the linear regressor. PCA is used with the sapphire dataset as the sapphire patterns contain significantly more diffraction features, and PCA compresses the dataset to give more consistent results from the logistic regression fitting. This was done to best simulate the accuracy of the next random prediction given a random prior distribution, including class imbalance. Classifiers are never combined between model runs to avoid test leakage. For the task 2 (XPS regression), the same fitting procedure is followed using 50 estimators, due to the reduced combinatorics of the input dataset. Jupyter notebooks used for the correlative modeling are available with live data integration at <https://github.com/atomic-data-sciences/api-client/tree/main/examples>.

## Acknowledgement

This work was supported in part by SUPREME, one of seven centers in JUMP 2.0, a Semiconductor Research Corporation (SRC) program sponsored by DARPA. This work was also supported in part by the DMREF program of the National Science Foundation (NSF) through the Division of Materials Research (DMR) Awards No. 2324172 and 1921818.

## Supporting Information Available

Example of film and substrate RHEED patterns showing incomplete reconstruction and grain alignment; details of forward predictive inference for film composition on samples synthesized after model fitting.

## References

- (1) Kim, K. S.; Kwon, J.; Ryu, H.; Kim, C.; Kim, H.; Lee, E.-K.; Lee, D.; Seo, S.; Han, N. M.; Suh, J. M.; Kim, J.; Song, M.-K.; Lee, S.; Seol, M.; Kim, J. The fu-

- ture of two-dimensional semiconductors beyond Moore’s law. *Nature Nanotechnology* **2024**, *19*, 895–906, Publisher: Nature Publishing Group.
- (2) Maine, E.; Seegopaul, P. Accelerating advanced-materials commercialization. *Nature Materials* **2016**, *15*, 487–491, Publisher: Nature Publishing Group.
- (3) Hegde, V. I.; Borg, C. K. H.; Del Rosario, Z.; Kim, Y.; Hutchinson, M.; Antono, E.; Ling, J.; Saxe, P.; Saal, J. E.; Meredig, B. Quantifying uncertainty in high-throughput density functional theory: A comparison of AFLOW, Materials Project, and OQMD. *Physical Review Materials* **2023**, *7*, 053805.
- (4) Yang, R. X.; McCandler, C. A.; Andriuc, O.; Siron, M.; Woods-Robinson, R.; Horton, M. K.; Persson, K. A. Big Data in a Nano World: A Review on Computational, Data-Driven Design of Nanomaterials Structures, Properties, and Synthesis. *ACS Nano* **2022**, *16*, 19873–19891.
- (5) Deng, B.; Zhong, P.; Jun, K.; Riebesell, J.; Han, K.; Bartel, C. J.; Ceder, G. CHGNet as a pretrained universal neural network potential for charge-informed atomistic modelling. *Nature Machine Intelligence* **2023**, *5*, 1031–1041.
- (6) Chen, C.; Ong, S. P. A universal graph deep learning interatomic potential for the periodic table. *Nature Computational Science* **2022**, *2*, 718–728.
- (7) Batatia, I.; Kovács, D. P.; Simm, G. N. C.; Ortner, C.; Csányi, G. MACE: Higher Order Equivariant Message Passing Neural Networks for Fast and Accurate Force Fields. **2022**,
- (8) Merchant, A.; Batzner, S.; Schoenholz, S. S.; Aykol, M.; Cheon, G.; Cubuk, E. D. Scaling deep learning for materials discovery. *Nature* **2023**, *624*, 80–85, Number: 7990 Publisher: Nature Publishing Group.
- (9) Zeni, C. et al. MatterGen: a generative model for inorganic materials design. **2023**,



- (10) Lee, A.; Sarker, S.; Saal, J. E.; Ward, L.; Borg, C.; Mehta, A.; Wolverton, C. Machine learned synthesizability predictions aided by density functional theory. *Communications Materials* **2022**, *3*, 1–11, Publisher: Nature Publishing Group.
- (11) Choudhary, K.; DeCost, B.; Chen, C.; Jain, A.; Tavazza, F.; Cohn, R.; Park, C. W.; Choudhary, A.; Agrawal, A.; Billinge, S. J. L.; Holm, E.; Ong, S. P.; Wolverton, C. Recent advances and applications of deep learning methods in materials science. *npj Computational Materials* **2022**, *8*, 59.
- (12) Delgado-Licona, F.; Abolhasani, M. Research Acceleration in Self-Driving Labs: Technological Roadmap toward Accelerated Materials and Molecular Discovery. *Advanced Intelligent Systems* **2023**, *5*, 2200331.
- (13) Szymanski, N. J.; Zeng, Y.; Huo, H.; Bartel, C. J.; Kim, H.; Ceder, G. Toward autonomous design and synthesis of novel inorganic materials. *Materials Horizons* **2021**, *8*, 2169–2198.
- (14) Xie, Y.; Sattari, K.; Zhang, C.; Lin, J. Toward autonomous laboratories: Convergence of artificial intelligence and experimental automation. *Progress in Materials Science* **2023**, *132*, 101043.
- (15) Szymanski, N. J. et al. An autonomous laboratory for the accelerated synthesis of novel materials. *Nature* **2023**, *624*, 86–91.
- (16) Lunt, A. M.; Fakhruddin, H.; Pizzuto, G.; Longley, L.; White, A.; Rankin, N.; Clowes, R.; Alston, B.; Gigli, L.; Day, G. M.; Cooper, A. I.; Chong, S. Y. Modular, multi-robot integration of laboratories: an autonomous workflow for solid-state chemistry. *Chemical Science* **2024**, *15*, 2456–2463.
- (17) Biswas, A.; Liu, Y.; Creange, N.; Liu, Y.-C.; Jesse, S.; Yang, J.-C.; Kalinin, S. V.; Ziatdinov, M. A.; Vasudevan, R. K. A dynamic Bayesian optimized active recommender

- system for curiosity-driven partially Human-in-the-loop automated experiments. *npj Computational Materials* **2024**, *10*, 29.
- (18) Ding, L.; Zhang, C.; Nærland, T. U.; Faleev, N.; Honsberg, C.; Bertoni, M. I. Silicon Minority-carrier Lifetime Degradation During Molecular Beam Heteroepitaxial III-V Material Growth. *Energy Procedia* **2016**, *92*, 617–623.
- (19) Hasegawa, S. *Characterization of Materials*; 2012; pp 1–14, eprint: <https://onlinelibrary.wiley.com/doi/pdf/10.1002/0471266965.com139>.
- (20) Liang, H.; Stanev, V.; Kusne, A. G.; Tsukahara, Y.; Ito, K.; Takahashi, R.; Lippmaa, M.; Takeuchi, I. Application of machine learning to reflection high-energy electron diffraction images for automated structural phase mapping. *Physical Review Materials* **2022**, *6*, 063805, Publisher: American Physical Society.
- (21) Vasudevan, R. K.; Tselev, A.; Baddorf, A. P.; Kalinin, S. V. Big-Data Reflection High Energy Electron Diffraction Analysis for Understanding Epitaxial Film Growth Processes. *ACS Nano* **2014**, *8*, 10899–10908, Publisher: American Chemical Society.
- (22) Kwoen, J.; Arakawa, Y. Classification of Reflection High-Energy Electron Diffraction Pattern Using Machine Learning. *Crystal Growth & Design* **2020**, *20*, 5289–5293, Publisher: American Chemical Society.
- (23) Gliebe, K.; Sehirlioglu, A. Distinct thin film growth characteristics determined through comparative dimension reduction techniques. *Journal of Applied Physics* **2021**, *130*, 125301.
- (24) Yang, J.-H.; Kang, H.; Kim, H. J.; Kim, T.; Ahn, H.; Rhee, T. G.; Khim, Y. G.; Choi, B. K.; Jo, M.-H.; Chang, H.; Kim, J.; Chang, Y. J.; Lee, Y.-L. <https://2DMat.ChemDX.org>: Experimental data platform for 2D materials from synthesis to physical properties. *Digital Discovery* **2024**, *3*, 573–585.

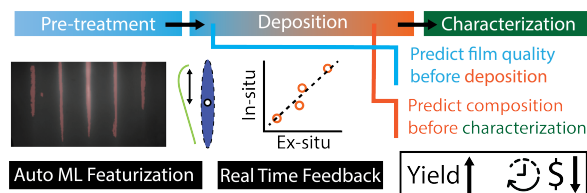
- (25) Provence, S. R.; Thapa, S.; Paudel, R.; Truttmann, T. K.; Prakash, A.; Jalan, B.; Comes, R. B. Machine learning analysis of perovskite oxides grown by molecular beam epitaxy. *Physical Review Materials* **2020**, *4*, 083807, Publisher: American Physical Society.
- (26) Kim, H. J.; Chong, M.; Rhee, T. G.; Khim, Y. G.; Jung, M.-H.; Kim, Y.-M.; Jeong, H. Y.; Choi, B. K.; Chang, Y. J. Machine-learning-assisted analysis of transition metal dichalcogenide thin-film growth. *Nano Convergence* **2023**, *10*, 10.
- (27) Zhang, F. et al. Monolayer Vanadium-Doped Tungsten Disulfide: A Room-Temperature Dilute Magnetic Semiconductor. *Advanced Science* **2020**, *7*, 2001174, eprint: <https://onlinelibrary.wiley.com/doi/pdf/10.1002/advs.202001174>.
- (28) Yun, S. J.; Duong, D. L.; Ha, D. M.; Singh, K.; Phan, T. L.; Choi, W.; Kim, Y.-M.; Lee, Y. H. Ferromagnetic Order at Room Temperature in Monolayer WSe<sub>2</sub> Semiconductor via Vanadium Dopant. *Advanced Science* **2020**, *7*, 1903076, eprint: <https://onlinelibrary.wiley.com/doi/pdf/10.1002/advs.201903076>.
- (29) Kirillov, A.; Mintun, E.; Ravi, N.; Mao, H.; Rolland, C.; Gustafson, L.; Xiao, T.; Whitehead, S.; Berg, A. C.; Lo, W.-Y.; Dollár, P.; Girshick, R. Segment Anything. 2023; <http://arxiv.org/abs/2304.02643>, arXiv:2304.02643 [cs].
- (30) Ma, J.; He, Y.; Li, F.; Han, L.; You, C.; Wang, B. Segment anything in medical images. *Nature Communications* **2024**, *15*, 654, Publisher: Nature Publishing Group.
- (31) Mortelmans, W.; Kazzi, S. E.; Mehta, A. N.; Vanhaeren, D.; Conard, T.; Meersschaut, J.; Nuytten, T.; Gendt, S. D.; Heyns, M.; Merckling, C. Peculiar alignment and strain of 2D WSe<sub>2</sub> grown by van der Waals epitaxy on reconstructed sapphire surfaces. *Nanotechnology* **2019**, *30*, 465601, Publisher: IOP Publishing.
- (32) He, L.; Wang, S. L.; Yang, J. R.; Yu, M. F.; Wu, Y.; Chen, X. Q.; Fang, W. Z.;

Qiao, Y. M.; Gui, Y.; Chu, J. Molecular beam epitaxy (MBE) in situ high-temperature annealing of HgCdTe. *Journal of Crystal Growth* **1999**, *201-202*, 524–529.

(33) Peng, L.-M. Electron Scattering Factors of Ions and their Parameterization. *Acta Crystallographica Section A: Foundations of Crystallography* **1998**, *54*, 481–485, Publisher: International Union of Crystallography.

(34) Kawamura, T.; Fukaya, Y.; Fukutani, K. Finding RHEED conditions sensitive to hydrogen position on Pd(100). *Surface Science* **2022**, *722*, 122098.

(35) Pawlak, J.; Przybylski, M.; Mitura, Z. An Analysis of Kikuchi Lines Observed with a RHEED Apparatus for a TiO<sub>2</sub>-Terminated SrTiO<sub>3</sub> (001) Crystal. *Materials* **2021**, *14*, 7077.



For Table of Contents Only

# Supporting Information: Predicting and Accelerating Nanomaterials Synthesis Using Machine Learning Featurization

Christopher C. Price,<sup>\*,†</sup> Yansong Li,<sup>‡</sup> Guanyu Zhou,<sup>‡</sup> Rehan Younas,<sup>‡</sup> Spencer S. Zeng,<sup>†</sup> Tim H. Scanlon,<sup>†</sup> Jason M. Munro,<sup>\*,†</sup> and Christopher L. Hinkle<sup>\*,‡</sup>

<sup>†</sup>*Atomic Data Sciences, Boston, Massachusetts 02116, United States*

<sup>‡</sup>*Department of Electrical Engineering, University of Notre Dame, Notre Dame, Indiana 46556, United States*

E-mail: chris@atomicdatasciences.com; jason@atomicdatasciences.com; chinkle@nd.edu

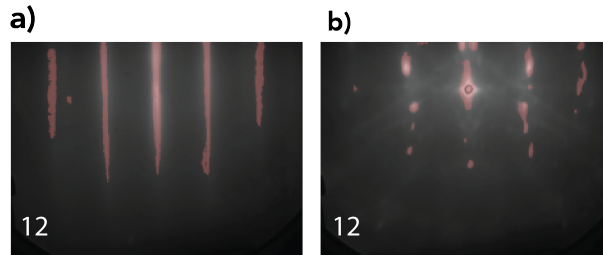


Figure S1: Zoomed-in view of an aligned growth which demonstrated a lower probability of classification. The substrate RHEED (b) shares features of both strongly predicted aligned and textured examples in Fig. 2d and small texturing features are visible in the film RHEED (a), consistent with the lower probability of the aligned prediction.

## Predictive Sample Inference

We tested the forward generalizability of all three inference models on a freshly prepared  $W_{1-x}V_xSe_2$  sample grown 3 months after the latest sample data and 3.5 years after the

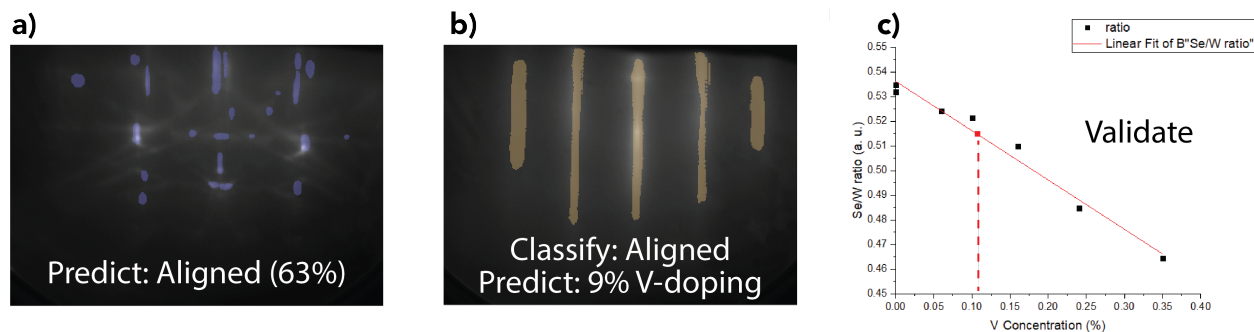


Figure S2: (a) Inference results using the models from Fig. 2 and Fig. 3c on the most recent set of substrate and film data, collected 3.5 years after the earliest sample in the training set.

earliest sample data used to develop the models in this study, without retraining the core featurization scheme or any of the correlative models (Fig. S2). This removes any implicit bias introduced in the train, test, and hyperparameter optimization, and extends the method application to clean synthesis. From the substrate RHEED data alone, our inference scheme predicted that aligned growth would be achieved with 63% probability. Inference from our film quality classifier on the deposited film matched this prediction and was verified by visual inspection of the deposited film RHEED. The same RHEED features across two angles were given to the compositional regression model, with the two RHEED angle predictions averaging to a predicted doping level of  $x=0.09$ . Subsequent XPS analysis for testing gave a manual composition of  $x=0.11$ . Points are plotted in conjunction with the original training and testing data in Fig. ??c. Without modifying any data infrastructure, all of the predictions were made within 15 seconds of RHEED capture, indicating this framework can provide real-time feedback within the timescales of dynamic advanced materials synthesis.